Acoust. Sci. & Tech. **34**, 1 (2013)

PAPER

Numerical evaluation of three-dimensional sound intensity measurement accuracies and a proposal for an error correction method

Takeshi Iino*, Hirokazu Tatekawa, Hisanobu Mizukawa and Hideo Suzuki

A&D Company, Limited, 1–243 Asahi, Kitamoto, 364–8585 Japan

(*Received 9 May 2012, Accepted for publication 23 August 2012*)

Abstract: In the three-dimensional (3-D) sound intensity measurement using four-microphone probes, there are two well-known microphone arrangements. One is arranging four microphones at the vertexes of a regular tetrahedron and the other is arranging them at the nearest four corners of a cube. In the high frequency region, these 3-D probes suffer from the same type of sensitivity reductions as do 1-D p-p probes. In this paper, formulae to obtain three orthogonal intensity components for these two types of probes are reviewed first, and their sensitivity and leakage errors are numerically discussed not only for the along-the-axis plane wave incidences but also for incidences from various directions in the 4π space. This analysis reveals characteristic differences of measurement errors of the two types of probes. Since the sensitivity and leakage errors are systematic, it is possible to correct these errors (to some degree) using the source direction information given by a real (or a numerical) measurement. A new correction method is proposed, and the effectiveness of the method is evaluated numerically. Results show that the proposed method is very effective, and the high-end of the frequency range is widened close to the limit, at which the dimension of the 3-D probe is nearly equal to the half wavelength of the incident plane wave.

Keywords: Sound intensity, Three dimensional sound intensity, Sensitivity correction, Intensity probe

PACS number: 43.58.+z [doi:10.1250/ast.34.34]

1. INTRODUCTION

Sound intensity (SI) is the sound energy flow per unit time and unit area. It is used for sound power measurements, sound source locations, and visualizations of sound fields [1–4]. The time-averaged SI is suitable for the sound power measurement, whereas the envelope intensity is recommended for the analysis of transient sounds [5–7].

The most common time-averaged and envelope intensity measurement methods are to use two (pressure) microphones (p-p probe) [1–3]. By use of the p-p probe, average sound pressure and particle velocity, and then time-averaged and/or envelope intensities at the center of the pair microphones are obtained. The three-dimensional (3-D) SI probe enables the simultaneous measurement of 3-D SI components, which is a must for SI measurements of transient sounds [8–13].

Use of cardioid type microphones has also been proposed for the measurement of sound intensities [14,15]. In this paper, however, only 3-D intensity methods using p-p probes are considered.

*e-mail: takeshi-iino@aandd.co.jp

The p-p probe has performance limitations in the low- and high-frequency regions. A phase mismatch between the two microphones causes the measurement error in the low-frequency region. The finite spacing (d) of the two microphones causes the approximation errors of the pressure and the particle velocity, resulting in the sensitivity reduction in the high-frequency region. If $d/\lambda \geq 0.184$ (λ: wavelength), the sensitivity reduction is 1 dB or larger. For example, if the highest measurement frequency is 2.5 kHz (or 10 kHz), d cannot exceed 25.2 mm (or 6.3 mm), which imposes severe restrictions on the selection of microphones and the design of probes. Also, making d smaller has an adverse effect on the phase mismatch errors in the low frequency region.

As stated before, for the analysis of a transient sound in the 3-D space, a 3-D intensity probe with at least four microphones is necessary [8–13]. Three pairs of p-p probes with six microphones proposed in Refs. [8] and [12] are arranged along the x-, y-, and z-axes, respectively. This arrangement is ideal in the sense that each of the orthogonal components is directly obtained from each pair of microphones, and the measurement positions of the three pairs can be set at the common origin of the coordinate

system. However, arranging six microphones in a narrow space makes the probe very clumsy, raising a concern of the sound field disturbance. The larger number of channels compared to the four-microphone probes are also cost-wise ineffective. For these reasons, only four-microphone 3-D probes will be discussed in this paper.

In the 3-D intensity measurement using four-microphone probes, there are two well-known microphone arrangements, i.e., arranging four microphones at vertexes of a regular tetrahedron [9–11] and at nearest four corners of a cube [13]. In the previous papers, the basic (i.e., theoretical or numerical) discussions of errors for these probes are mostly limited to wave incidences along the three orthogonal axes. In this paper, the measurement errors of these two types of probes for various incident angles in the 4π space are numerically discussed. Because of the symmetry between the front and rear 2π spaces, only the front 2π space is evaluated.

Since the sensitivity reduction error is systematic, it can be corrected if the direction of SI is known or at least roughly estimated. In Ref. [11], the cross-spectra of pairs of microphones are modified in the frequency domain using directional information of the initial 3-D SI measurement.

The present paper first reviews the derivation of formulae to obtain intensities of three orthogonal axis components for two types of four-microphone 3-D intensity probes. Second, errors in the high frequency range caused by the finite approximation are discussed for various directions of plane wave incidence. Finally, a new error correction method that can be applied to both time-averaged and envelope intensities is proposed and its effectiveness is discussed. A practical object of this paper is to extend the frequency range up to 2.5 kHz (or 10 kHz) using a probe with $L_x = 60$ mm (or 16 mm), which is very close to the half wavelength of a 2.5 kHz (or 10 kHz) plane wave (see Fig. 2 for L_x).

2. REVIEW OF 1-D INTENSITY MEASUREMENT BY THE USE OF P-P INTENSITY PROBES

By the use of a p-p probe, two pressures $p_1(t)$ and $p_2(t)$ are measured at two points (assumed to be both on the x-axis for simplicity) with spacing d between them in the free space. Then the pressures at the center of the probe in the time and frequency domains are given, respectively, by

$$\begin{aligned} p(t) &= [p_1(t) + p_2(t)]/2 \\ P(f) &= [P_1(f) + P_2(f)]/2 \end{aligned} \tag{1}$$

The particle velocities in the direction of measurement are given, respectively, by

$$\begin{aligned} u(t) &= -(1/\rho)\int_{-\infty}^{t} [\partial p(t')/\partial x]dt' \\ U(f) &= [P_1(f) - P_2(f)]/j2\pi f\rho d \end{aligned} \tag{2}$$

where ρ is the air density. The instantaneous SI is defined by

$$I_i(t) = p(t)u(t) \tag{3}$$

The time-averaged SI is defined by

$$I_a = \left((1/T)\int_{-T/2}^{T/2} I_i(t)dt\right)_{T\to\infty} \tag{4}$$

For a 1-D plane wave without reflection, Eq. (4) becomes

$$I_a = P^2/\rho c \tag{5}$$

where P is the rms pressure amplitude and c is the sound velocity. The time-averaged SI can also be defined using the cross-spectrum $S_{pu}(f)$ between $p(t)$ and $u(t)$ by

$$I_a = \mathrm{Re}\left[\int_{-\infty}^{\infty} S_{pv}(f)df\right] \tag{6}$$

Applying the p-p probe, Eq. (6) can be calculated using $p_1(t)$ and $p_2(t)$ by

$$I_a = -\int_0^{\infty} [\mathrm{Im}\{G_{p1p2}(f)\}/(2\pi f\rho d)]df \tag{7}$$

where $G_{p1p2}(f)$ is the one-sided cross-spectrum between $p_1(t)$ and $p_2(t)$ [4]. The integrand is the intensity spectrum of time-averaged SI obtained by use of the p-p probe.

$$I_s(f) = -(1/2\pi f\rho d)\,\mathrm{Im}[G_{p1p2}(f)] \tag{8}$$

For the 1-D plane wave without reflection in the direction from the microphone 1 to 2, $p_1(t)$ and $p_2(t)$ are given, respectively, by

$$\begin{aligned} p_1(t) &= \sqrt{2}P\cos\{2\pi ft + (kd/2)\cos(\alpha)\}, \\ p_2(t) &= \sqrt{2}P\cos\{2\pi ft - (kd/2)\cos(\alpha)\} \end{aligned} \tag{9}$$

where $\cos(\alpha)$ is the directional cosine between the wave propagation and the direction of the microphone pair (from 1 to 2). Applying Eq. (9) to Eq. (8), $I_s(f)$ is given by

$$I_s(f) = (P^2/\rho c)\cos(\alpha)\frac{\sin[(2\pi f/c)d\cos(\alpha)]}{(2\pi f/c)d\cos(\alpha)} \tag{10}$$

The envelope intensity is defined similarly as Eq. (3) by

$$I_e(t) = \mathrm{Re}[p_a{}^*(t)u_a(t)] \tag{11}$$

where $p_a(t)$ and $u_a(t)$ are analytic signals of $p(t)$ and $u(t)$, respectively, and the symbol "*" indicates a complex conjugate. An "analytic" signal is defined as a signal that has only positive frequency components. As Eq. (11) shows, the pressure and the particle velocity must be handled separately in the time domain.

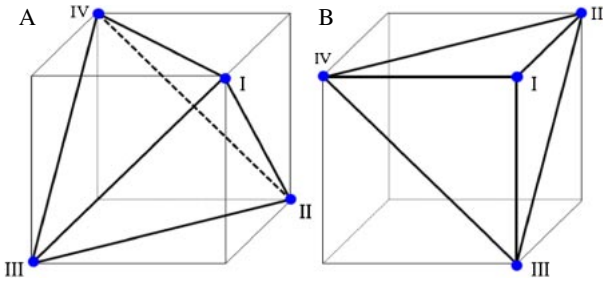

Fig. 1 Two types of four-microphone arrangement.

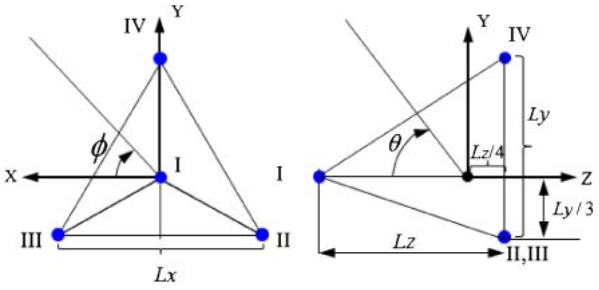

Fig. 2 Four-microphone probe and its coordinate system.

3. PRINCIPLE OF 3-D INTENSITY MEASUREMENT

3.1. Geometries of Four-Microphone Probes

Two types of four-microphone arrangements have been reported. One of them is to arrange the microphones as shown in Fig. 1(A), where a set of four vertexes of a regular hexahedron that compose a regular tetrahedron is used [9–11]. In the other arrangement, as shown in Fig. 1(B), one reference vertex and three other nearest vertexes of a cube (regular hexahedron) are used [13]. In both arrangements, microphones II, III, and IV compose a regular triangle. These two probes are referred to as "type A probe" and "type B probe," respectively.

The coordinate system of these probes may be taken as shown in Fig. 2. The origin of the coordinate system is set at the centroid of the tetrahedron, the line of the microphone pair II–III is parallel to the x-axis, and the z-axis is referred to as the "probe axis." The bottom triangle is parallel to the x-y plane (i.e., perpendicular to the z-axis). For both probes, $L_y = (3/4)^{1/2}L_x$. For type A probe $L_z = (2/3)^{1/2}L_x$, and for type B probe, $L_z = 6^{-1/2}L_x$ (one-half of type A). The angles φ and θ are azimuth and zenith angles, respectively (note that θ starts from the negative z-axis).

3.2. Time-Averaged SI Spectrum

3.2.1. Type A probe

For the type A probe, formulae given in Ref. [10] are cited here first with a slightly modified form.

$$
\begin{aligned}
I_{s,x} &= \frac{1}{2\pi f\rho L_x}\frac{1}{4}\,\mathrm{Im}[-G_{12}+G_{13}+2G_{23}+G_{24}-G_{34}] \\
I_{s,y} &= \frac{1}{2\pi f\rho L_y}\frac{1}{8}\,\mathrm{Im}[-G_{12}-G_{13}+2G_{14} \\
&\quad +3G_{24}+3G_{34}] \\
I_{s,z} &= \frac{1}{2\pi f\rho L_z}\frac{1}{3}\,\mathrm{Im}[G_{12}+G_{13}+G_{14}]
\end{aligned}
\tag{12}
$$

In Ref. [10], Eq. (12) is obtained through the following rather lengthy process:

(1) Calculate the average pressure at the centroid.

(2) Calculate the four particle velocity component using each of the four pressures and the average pressure at the centroid.

(3) Convert them to particle velocities in the direction parallel to the x-, y-, and z-axes.

(4) Obtain real parts of the cross-spectra between the average pressure and each component of the particle velocities along the x-, y-, and z-axes.

Another method to obtain Eq. (12) is given here. The SI spectra in the x-direction obtained by the pair microphones are given, respectively, by

$$
\begin{aligned}
I_{s,x,12} &= -\mathrm{Im}[G_{12}]/[2\pi f\rho(L_x/2)] \\
&= -\mathrm{Im}[G_{12}\cdot 2]/[2\pi f\rho L_x] \\
I_{s,x,13} &= +\mathrm{Im}[G_{13}]/[2\pi f\rho(L_x/2)] \\
&= +\mathrm{Im}[G_{13}\cdot 2]/[2\pi f\rho L_x] \\
I_{s,x,23} &= +\mathrm{Im}[G_{23}]/[2\pi f\rho(L_x)] \\
&= +\mathrm{Im}[G_{23}]/[2\pi f\rho L_x] \\
I_{s,x,24} &= +\mathrm{Im}[G_{24}]/[2\pi f\rho(L_x/2)] \\
&= +\mathrm{Im}[G_{24}\cdot 2]/[2\pi f\rho L_x] \\
I_{s,x,34} &= -\mathrm{Im}[G_{34}]/[2\pi f\rho(L_x/2)] \\
&= -\mathrm{Im}[G_{34}\cdot 2]/[2\pi f\rho L_x]
\end{aligned}
\tag{13}
$$

The time-averaged SI spectra in the x-direction can be obtained by taking average with weights (1: 1: 2^2: 1: 1), which are the squares of ratios of the effective length in the x-direction, resulting in

$$
\begin{aligned}
I_{s,x} &= \frac{1}{2\pi f\rho L_x}\frac{1}{8}\,\mathrm{Im}[-1\cdot 2G_{12}+1\cdot 2G_{13}+4 \\
&\quad \cdot 1G_{23}+1\cdot 2G_{24}-1\cdot 2G_{34}] \\
&= \frac{1}{2\pi f\rho L_x}\frac{1}{4}\,\mathrm{Im}[-G_{12}+G_{13}+2G_{23}+G_{24}-G_{34}]
\end{aligned}
\tag{14}
$$

which is identical with the first equation of Eq. (12). In the same manner, the SI spectra in the y- and z-directions, are given as those in Eq. (12). Considering the method of derivation of Eq. (14), it is clear that Eq. (12) can also be applied to any probe given in Fig. 2 with an arbitrary height (L_z).

In Ref. [9], the three axes of the coordinate system are taken parallel to the corresponding sizes of the cube, and the centroid is taken at the center of the cube, which coincides with the origin of Fig. 2. It was confirmed that by rotating the coordinate system, Eq. (12) is obtained from the formula given in Ref. [9] and vice versa.

3.2.2. Type B probe

For the type B probe, microphone pairs I–II, I–III, and I–IV will be used for the measurement of the three orthogonal SI components. The time-averaged SI spectra obtained using those pairs are given by

$$\begin{Bmatrix} I_{s,1} \\ I_{s,2} \\ I_{s,3} \end{Bmatrix} = \begin{Bmatrix} \mathrm{Im}[G_{12}]/[2\pi f\rho L_x/\sqrt{2}] \\ \mathrm{Im}[G_{13}]/[2\pi f\rho L_x/\sqrt{2}] \\ \mathrm{Im}[G_{14}]/[2\pi f\rho L_x/\sqrt{2}] \end{Bmatrix} \tag{15}$$

If the x-, y-, and z-axes are taken along the microphone pairs I–II, I–III, and I–IV, respectively, the three orthogonal components are directly given by Eq. (15). However, the coordinate system given in Fig. 2 may be more natural for the tetrahedron type microphone arrangement.

Using the direction cosines between the directions of the microphone pairs and the three axes (Fig. 2), the time-averaged SI spectra $\{I_x\ I_y\ I_z\}$ measured on the x, y, and z-axes can be converted from those measured by the orthogonal microphone pairs by

$$\begin{Bmatrix} I_{s,x} \\ I_{s,y} \\ I_{s,z} \end{Bmatrix} = \begin{bmatrix} -1/\sqrt{2} & 1/\sqrt{2} & 0 \\ -1/\sqrt{6} & -1/\sqrt{6} & 2/\sqrt{6} \\ 1/\sqrt{3} & 1/\sqrt{3} & 1/\sqrt{3} \end{bmatrix} \begin{Bmatrix} I_{s,1} \\ I_{s,2} \\ I_{s,3} \end{Bmatrix} \tag{16}$$

or

$$\begin{aligned} I_{s,x} &= \frac{1}{2\pi f\rho L_x}\mathrm{Im}[-G_{12}+G_{13}] \\ I_{s,y} &= \frac{1}{2\pi f\rho L_y}\frac{1}{2}\mathrm{Im}[-G_{12}-G_{13}+2G_{14}] \\ I_{s,z} &= \frac{1}{2\pi f\rho L_z}\frac{1}{3}\mathrm{Im}[G_{12}+G_{13}+G_{14}] \end{aligned} \tag{17}$$

Note, however, that Eqs. (16) and (17) require the condition that the measurement points of intensity components $I_{s,j}$ $(j=1,2,3)$ are identical. This condition is satisfied in the case of a plane wave, since the direction cosines are not affected by the relative positions of the three microphone pairs (only their directions matter).

4. MEASUREMENT ERRORS

There are two types of finite difference approximation errors. The first one is the sensitivity reduction error, and the second is the leakage error. Additionally, as a result of these errors, an estimated direction of energy flow at the measurement point is shifted from the true direction of the energy flow. For a point source in a free space, since the direction of the energy flow is identical with the direction of the source, this will be simply referred to as the "source direction estimation error." In the numerical evaluation of errors, the probe sizes of type A and B probes are fixed with $L_x = 60$ mm. Type A and B probes are paired with Eqs. (12) and (17), respectively, unless otherwise mentioned.

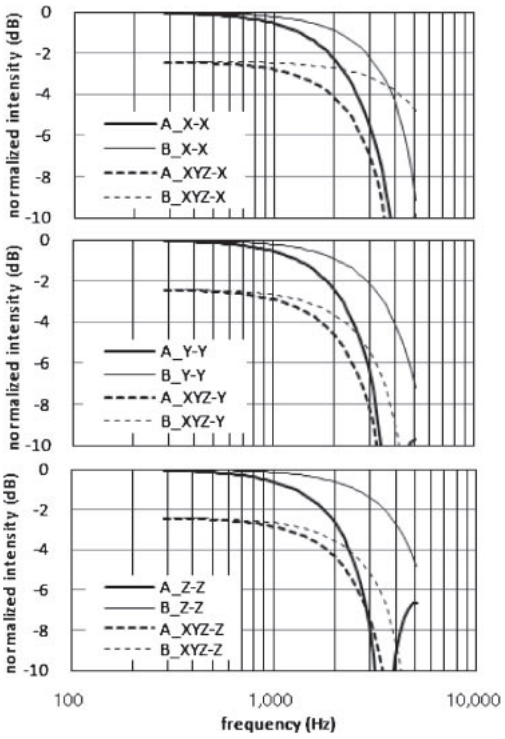

Fig. 3 Sensitivity characteristics of type A and B probes with $L_x = 60$ mm for the four incidence angles.

4.1. Sensitivity Reduction Errors

The sensitivity reduction error for a 1-D probe can be defined using Eq. (10) by

$$SRE = \frac{\sin[(2\pi f/c)d\cos(\alpha)]}{(2\pi f/c)d\cos(\alpha)} = \frac{\sin[\{2\pi d\cos(\alpha)\}/\lambda]}{\{2\pi d\cos(\alpha)\}/\lambda} \tag{18}$$

This is a systematic error, which is caused by the finite difference approximations given by Eqs. (1) and (2) [4]. At frequencies that satisfy the condition, $d\cos(\alpha)/\lambda \geq 0.184$, the sensitivity reduction exceeds 1 dB. 3-D probes that are composed of 1-D probes have similar sensitivity reductions.

Figure 3 shows sensitivity characteristics of type A and type B probes when a plane wave propagates in the x-, y-, and z-directions and also in the direction with the same direction cosines $1/3^{1/2}$ with the three axes (indicated by '*xyz*' in the figures). For example, A_XYZ-Y indicates the sensitivity of the type A probe in the y-direction for the wave propagating in the *xyz*-direction. Note that intensities are normalized to the intensity of the plane wave, $P^2/\rho c$.

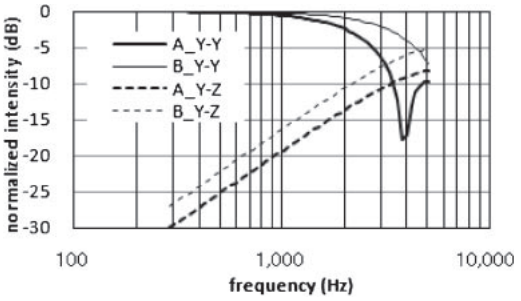

Fig. 4 Leakage errors of type A and type B probes with $L_x = 60$ mm.

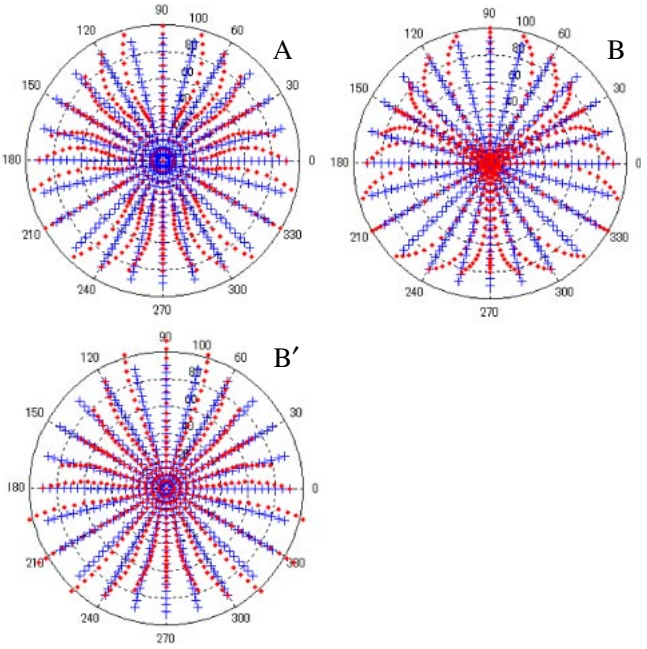

Fig. 5 True and estimated source directions of a 2.5 kHz plane for type A, B, and B′ probes. See Fig. 2 for the azimuth ($\phi = 0°$–$360°$) and zenith ($\theta = 0°$–$100°$) angles. (MATLAB polar coordinate function "polar" is used to draw Figs. 5 and 8.)

The results show that the type B probe has better sensitivity (less sensitivity reduction) than the type A probe. This is because the height of the type B probe is half of the type A probe. If the intensity measurement error within 1 dB is a measurement criterion, the highest frequency is approximately 1.3 kHz and 2 kHz for type A and type B probes, respectively. This indicates that the type B probe is preferable in extending the measurement frequency range as far as these four incident angles are concerned.

4.2. Leakage Errors

Another type of measurement error is leakage, which can be defined as an extraneous SI measured on one axis when a plane wave propagates along another orthogonal axis. It is known that, in the type A probe, the leakage exists in the z-axis when the wave propagation is along the y-axis [10]. There is no leakage when the wave propagates along the x- or z-axis. This is also true for type B probe.

The curves A_Y-Z and B_Y-Z in Fig. 4 show leakage errors in the z-axis when a plane wave propagates along the y-axis. There is a 3 dB difference between the leakages of type A and B probes. This is because the cross-spectra included in the third equations of Eqs. (12) and (17) are the same for the y-axis plane wave incidence, and those are divided by L_z ($= 0.82\,L_x$ for type A and $0.41\,L_x$ for type B). For both probes, the leakage is approximately -10 dB below the measured y-axis components at 2 kHz. The leakage error is also a limiting factor of the performance of 3-D intensity probes.

In a wider sense, the leakage should be defined for any incident angle. If the ratios of measured orthogonal intensity components change from the true ratios, it may be the result of a leakage error. This type of error is discussed next.

4.3. Source Direction Estimation Errors

The directions of the plane wave propagation (in other words, directions of a far-away point source in the free space) considered in the previous two subsections were along the three axes and the source direction with the identical directional cosines, $1/3^{1/2}$, with the three axes. In practical situations, the source can be everywhere, and therefore, the error should be evaluated for arbitrary sound wave incident angles.

In order to evaluate the source direction estimation errors over the 2π space, the source location is varied using the azimuth angle φ and the zenith angle θ (see Fig. 2). Figure 5(A) and (B) show true and estimated source directions for type A and type B probes for a 2.5 kHz plane wave (2.5 kHz is the target frequency for $L_x = 60$ mm). The azimuth angle φ is varied from 0° to 360° in 15° steps. The zenith angle θ is varied from 0° to 90° in 5° steps (total of 433 points). The patterns of the source direction estimation errors for the rear hemispherical surface are obtained by reversing the respective front patterns with respect to the 0°–180° line. The patterns are symmetric with respect to the 30°–210°, 90°–270°, and 150°–330° lines as expected from the microphone arrangements under consideration. Note that an estimated source direction is the same as the true source direction if there is only the sensitivity reduction (i.e., no leakage in the wide sense). Note also that the same amount of error is displayed larger as the zenith angle θ gets closer to 90°.

The type A probe has smaller discrepancies between the straight radial lines shown by "×" (true source directions) and the curved lines shown by "•" (estimated source directions), indicating that type A probe is better in

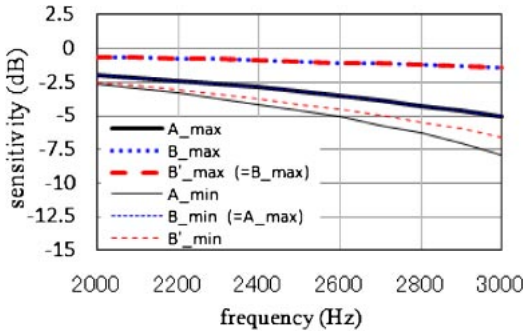

Fig. 6 Maximum and minimum normalized intensities of type A, B, and B′ probes obtained when the source direction is varied over the 433 points in the 2π space.

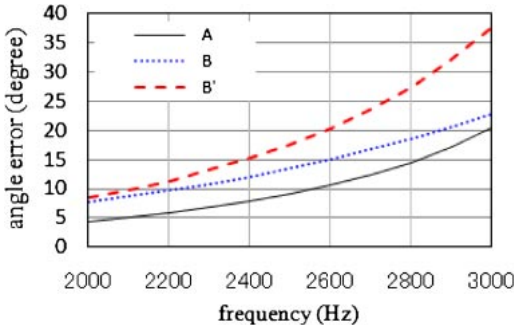

Fig. 7 Maximum angle differences between the true and estimated source directions obtained when the source direction is varied over the 433 points in the 2π space.

estimating source directions. The type A probe has larger sensitivity reductions but smaller leakage errors compared to the type B probe. Complexity of the patterns in Fig. 5 indicates that the errors must be evaluated for various source directions.

As mentioned before, Eq. (12) can be applied to the type B probe, which is referred to as a type B′ probe. Figure 5(B′) shows the true and estimated source directions obtained for this combination. The degree of shift from the true to the estimated source directions in the circumferential direction of Fig. 5(B′) is much smaller than that of Fig. 5(B). On the other hand, those shifts in the radial directions of Fig. 5(B′) are larger than those of Fig. 5(A) and (B).

Another way of comparing the degrees of errors of the probes is to look for maximum and minimum intensities among the intensities obtained at the 433 evaluation points in the 2π space and also look for a maximum angle difference between the true and the estimated source directions.

Figure 6 shows maximum and minimum normalized intensities for the three types of probes in the frequency range from 2 kHz to 3 kHz. The type A probe has the smallest maximum and minimum intensities, but the difference between them is minimum, which indicates that the source direction estimation errors are smaller than for type B and B′ probes. Type B and B′ probes have the same maximum intensities but the latter has smaller minimum intensities than the former. At first glance Fig. 5 gives us an impression that the type B′ probe is better than the type B probe. However, since large errors are on the 30°–210°, 90°–270°, and 150°–330° radial lines, it is difficult to visually evaluate magnitudes of errors on these lines.

Figure 7 shows maximum angle differences between the true and estimated source directions among the angle differences obtained at 433 points in the frequency range from 2 kHz to 3 kHz. The results clearly show that the type A probe has smaller source direction estimation errors than type B and B′ probes. The maximum angle differences are observed on the 30°–210°, 90°–270°, and 150°–330° lines for all types of probes.

Without comparisons of such patterns as those given in Fig. 5 and maximum and minimum values as given in Figs. 6 and 7, it will be very difficult to evaluate degrees of errors of 3-D probes in the 2π space. As a whole, it can be said that the type A probe has larger sensitivity reductions but smaller leakages (i.e., source direction estimation errors) than the other two probes.

5. PROPOSAL OF A NEW ERROR CORRECTION METHOD AND ITS NUMERICAL EVALUATION

The sensitivity reduction errors and leakage errors are systematic, which means there is a possibility for error corrections. If the direction cosine ($\cos\alpha$) between the pair of microphones and the direction of the wave propagation is known, the sensitivity reduction can be corrected by applying Eq. (18) to each of cross-spectra in Eq. (12) or (17). This is the method adopted in Ref. [13], which works for the time-averaged SI measurement using the cross-spectrum method.

Another method is to prepare a mapping table between true and estimated sound source directions and intensities. If there is a detailed mapping table (in other words, obtained by dividing φ and θ into very small segments) between the measured source direction and its true source direction, the latter can be obtained from the former. However, since the tables must be prepared for a very large number of source directions and also for different frequencies, it becomes voluminous. A similar but effective and sufficient method is proposed here.

In a real measurement, an intensity magnitude $|I_1|$ and a source direction (φ_1, θ_1) are obtained from measured three intensity components I_{x1}, I_{y1}, and I_{z1} using the following equations:

$$|I_1| = \sqrt{{I_{x1}}^2 + {I_{y1}}^2 + {I_{z1}}^2}$$
$$\varphi_1 = \tan^{-1}(I_{y1}/I_{x1}), \quad \theta_1 = \tan^{-1}(\sqrt{{I_{x1}}^2 + {I_{y1}}^2}/I_{z1}) \tag{19}$$

These are different from the true intensity magnitude $|I_0|$ and the source direction (φ_0, θ_0). Assuming that a plane wave with 1 Pa rms amplitude comes from the measured direction (φ_1, θ_1), its intensity $|I_2|$ and source direction (φ_2, θ_2) are calculated by the use of Eq. (12) (type A) or Eq. (17) (type B). The shift of direction should be close to the shift from the original (true) source direction (φ_0, θ_0) to the measured source direction (φ_1, θ_1) as far as the degree of error is not too large, i.e.,

$$\varphi_0 - \varphi_1 \approx \varphi_1 - \varphi_2, \quad \theta_0 - \theta_1 \approx \theta_1 - \theta_2 \tag{20}$$

A similar relationship holds for the intensity magnitudes:

$$|I_0|/|I_1| \approx (1/\rho c)/|I_2| \tag{21}$$

Then, the true source direction and the true intensity magnitude can be approximated, respectively, by

$$\varphi_0 \approx 2\varphi_1 - \varphi_2, \quad \theta_0 \approx 2\theta_1 - \theta_2 \tag{22}$$

and

$$|I_0| \approx |I_1|/(\rho c/|I_2|) \tag{23}$$

Equations (22) and (23) can be used for the correction of the measurement error. Note that corrected intensities may become larger than true intensities if excessive corrections are made.

Figure 8 shows true source directions by the symbol "+" and their respective estimated source directions, after the proposed correction is applied, by symbol "•." Figure 8(A′) shows a magnified view of Fig. 8(A) in the range $0° \le \theta \le 30°$. By comparing Fig. 8 with Fig. 5, it is apparent that the proposed correction method is very effective. Figure 8(A′) shows that, if a source is on the circle with $\theta = 5°$, its estimated source is roughly on the circle with $\theta = 2.5°$ (2.5° error). Actually, this is close to the largest errors among the cases of the 433 source locations.

The largest and the smallest intensity magnitudes after the correction and after normalizing to the true intensity $(P^2/\rho c)$ are shown in Fig. 9 in the frequency range from 2 to 3 kHz. Note that the maximum sensitivity errors are zero for type A and B probes. Figure 9 shows that the sensitivity correction of the proposed method is also very effective. For the case of the type A probe, the sensitivity error is kept within +0 dB and −0.5 dB at 2.5 kHz, less than half the errors of type B and B′ probes.

Figure 10 shows the maximum angle differences between the true source direction and the estimated source direction after the correction. The type A probe is also much better than type B and B′ probes. For the case of the type A probe with $L_x = 60$ mm (or 15 mm), which has an intensity error within +0 dB and −0.37 dB and a source direction estimation error less than 3°, it can be said that the frequency range of the probe is extended to the target frequency of 2.5 kHz (or 10 kHz) by applying the proposed correction method. Since the type A probe is two times larger than the type B (and B′) probe in height, it is less vulnerable to phase mismatch errors in the low frequency region.

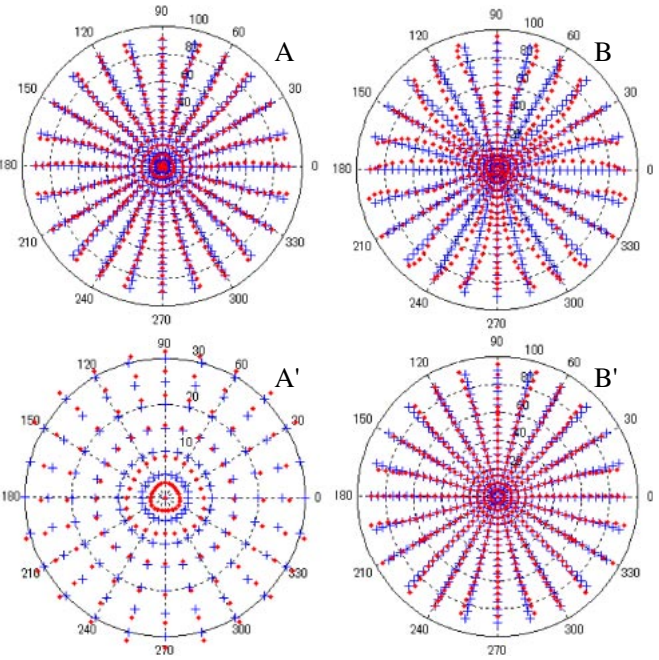

Fig. 8 True and estimated source directions for a 2.5 kHz plane wave by the use of type A, B, and B′ probes. The estimated source directions are those obtained after the correction. Figure 8(A′) shows a magnified view of Fig. 8(A) in the range $0° \le \theta \le 30°$. See Fig. 2 for the azimuth ($\phi = 0°$–$360°$) and zenith ($\theta = 0°$–$100°$) angles.

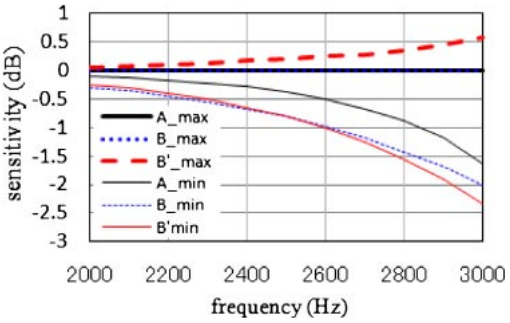

Fig. 9 Maximum and minimum sensitivity errors (after the correction) of type A, B, and B′ probes obtained when the source direction is varied over the 433 points in the 2π space.

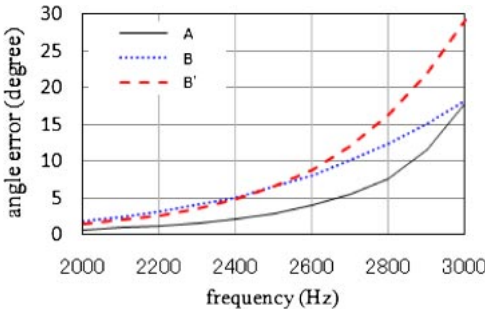

Fig. 10 Maximum angle differences after the correction between the true and estimated source directions obtained when the source direction is varied over the 433 points in the 2π space.

6. CONCLUSIONS

One of the well known four-microphone arrangements for 3-D intensity measurement is placing them at the vertexes of a regular tetrahedron (type A). The other uses a tetrahedron with one-half the height of the type A arrangement (i.e. type B).

The smaller probe (type B) had fewer sensitivity reduction errors when evaluated for the along-the-axis plane wave incidences. When evaluated over various source directions on the front 2π hemisphere, the type B probe suffered from larger leakage errors than the type A probe. The evaluation of the errors over the 2π space revealed characteristic differences of errors between the type A and type B probes.

An error correction method was proposed to reduce both the sensitivity and leakage errors. The effectiveness of the proposed method was also evaluated for various source directions in the 2π surface, and the results were excellent, especially for the type A probe. After the correction was applied, the type A probe had much smaller sensitivity reduction, leakage, and source direction estimation errors than the type B probe and its modified version. The target frequencies of 2.5 kHz for a 60 mm-size probe and 10 kHz for a 15 mm probe have been achieved. This is beneficial, since a larger probe is suited for reducing phase-mismatch errors in the low frequency region.

Since the proposed method does not need to correct each of the cross-spectra, it can be applied to narrow-band envelope intensities, in which three intensity components are given at any moment in the time domain.

In the present paper, measurement accuracies were evaluated only for plane wave fields. A preliminary study indicates effectiveness for fields with reflections and fields created by nearby point sources, confirmation of which remains for future research.

REFERENCES

[1] G. Pavic, "Measurement of sound intensity," *J. Sound Vib.*, **51**, 533–546 (1977).
[2] J. Y. Chung, "Cross-spectral method of measuring acoustic intensity," Research Publication, General Motors Research Laboratory, GMR-2617, Warren, Michigan (1977).
[3] F. J. Fahy, "Measurement of acoustic intensity using the cross-spectral density of two microphone signals," *J. Acoust. Soc. Am.*, **62**(L), 1057–1059 (1977).
[4] F. J. Fahy, *Sound Intensity* (Elsevier Applied Science, London/New York, 1989).
[5] H. Suzuki, M. Anzai, T. Ono and N. Suzuki, "An evaluation of a transient sound by an envelope intensity," *Proc. Annu. Meet. INCE/J*, pp. 325–328 (1990) (in Japanese).
[6] H. Suzuki, S. Oguro, M. Anzai and T. Ono, "A basic study of an envelope intensity," *Proc. Inter-noise 91*, Vol. 2, pp. 1037–1040 (1991).
[7] F. Jacobsen, "A note on instantaneous and time-averaged active and reactive sound intensity," *J. Sound Vib.*, **147**, 489–496 (1991).
[8] G. Rasmussen, "Measurement of vector sound fields," *Proc. 2nd Int. Congr. Acoustic Intensity*, pp. 53–58 (1985).
[9] L. M. S. Santos, C. C. Rodoregues and L. Bento Coelho, "Measuring the three-dimensional acoustic intensity vector with a four-microphone probe," *Proc. Inter-noise 89*, pp. 965–968 (1989).
[10] H. Suzuki, M. Anzai, S. Oguro and T. Ono, "Performance evaluation of a three dimensional intensity probe," *J. Acoust. Soc. Jpn.* (*E*), **16**, 233–238 (1995).
[11] H. Suzuki, S. Oguro and T. Ono, "A sensitivity correction method for a three-dimensional sound intensity probe," *Acoust. Sci. & Tech.*, **21**, 259–265 (2000).
[12] S. Nagata, K. Furihata, T. Wada, D. K. Asano and T. Yanagisawa, "A three-dimensional sound intensity measurement system for sound source identification and sound power determination by ln models," *J. Acoust. Soc. Am.*, **118**, 3691–3705 (2005).
[13] K. H. Miah and E. L. Hixon, "Design and performance evaluation of a broadband three dimensional acoustic intensity measuring system," *J. Acoust. Soc. Am.*, **127**, 2338–2346 (2010).
[14] S. Yokoyama, K. Ueno, S. Sakamoto and H. Tachibana, "6-channel recording/reproduction system for 3-dimensional auralization of sound fields," *Acoust. Sci. & Tech.*, **23**, 97–103 (2002).
[15] T. Hanyu, D. Inage and K. Sekiguchi, "Measurement of directional information of sound field by 4-channel cardioid microphones," *Proc. Spring Meet. Acoust. Soc. Jpn.*, pp. 1123–1126 (2008).